PAPER

Low loss and omnidirectional Si_3N_4 waveguide for label-free spatial frequency shift super-resolution imaging

View the article online for updates and enhancements.

IOP ebooks™

Bringing together innovative digital publishing with leading authors from the global scientific community.

Start exploring the collection–download the first chapter of every title for free.

Low loss and omnidirectional Si$_3$N$_4$ waveguide for label-free spatial frequency shift super-resolution imaging

Dehao Ye[1], Mingwei Tang[1], Xiaowei Liu[1,2], Yaoguang Ma[1], Xu Liu[1] and Qing Yang[1,2,3,*]

[1] State Key Lab of Modern Optical Instrumentation, College of Optical Science and Engineering,
International Research Center for Advanced Photonics, Zhejiang University, Hangzhou 310058,
People's Republic of China
[2] Research Center for Intelligent Sensing, Zhejiang Lab, Hangzhou 311100, People's Republic of China
[3] Collaborative Innovation Center of Extreme Optics, Shanxi University, Taiyuan 030006,
People's Republic of China

E-mail: qingyang@zju.edu.cn

Abstract

Waveguide-based spatial frequency shift (SFS) super-resolution imaging has attracted growing interest for its high integration, low cost and compatibility with integrated circuit processes. However, a missing band in the spatial frequency (SF) domain severely impedes the final distortionless super-resolution image reconstruction. Here, we present a tunable multi-wavelength SFS method that can light the sample with tunable wavelength illuminations in a sequence using multiple directions of waveguide illumination. The SFS scheme provides broad and complete spectrum information, enabling a reconstructed super-resolution image with high fidelity. An etched three-slot structure and randomly distributed polymer beads on the waveguide surface are imaged and reconstructed with a Gerchberg–Saxton (G-S) SF synthesis algorithm. To the best of our knowledge, this is the first report that shows the waveguide-based label-free super-resolution imaging capability of complex random samples. In the future, the novel SFS imaging waveguide can potentially be integrated with conventional microscopes for chip-based label-free super-resolution imaging.

Keywords: spatial frequency shift, Si$_3$N$_4$ waveguide, super-resolution imaging,
multi-wavelength evanescent illumination

(Some figures may appear in colour only in the online journal)

1. Introduction

Optical microscopy is an indispensable tool in many fields of scientific research, such as biomedicine and materials science. However, because of the Abbe diffraction limit, the resolution under conventional optical imaging systems is limited to the illumination wavelength (λ) and the numerical aperture (NA) of the objective lens. Subwavelength-size information is in the form of an evanescent wave which decays exponentially

with distance and cannot be captured in the far-field. In 2000, Pendry proposed a superlens, which was made of a thin slab of negative refractive index silver material. Through the plasmon-based evanescent wave enhanced in silver medium, it offered the possibility to restore the subwavelength information [1, 2]. Recently, it has been found that arbitrary materials filled in a bounded metallic waveguide can be used to build a low-loss superlens at the desired frequency, which breaks the conventional barriers of plasmon-based lens [3]. The hyperlens is another super-resolution imaging method. The hyperbolic anisotropic dispersion design used to realize the hyperlens is a cylindrical or spherical multilayer structure and

---

1

can achieve a resolution in the order of 70 nm [4]. Following this work, nonresonant waveguide-integrated hyperlens with a radially oriented layer structure was designed to resolve two nanoslits 250 nm apart with 780 nm wavelength [5, 6]. Additonally, microsphere lens [7], resonant metalenses [8] and super-oscillatory lens [9] also have the capability of surpassing the diffraction limit. It is significant for scientists to develop a perfect super-resolution imaging method, but these methods still face the limitations of a small field of view (FOV) and the difficulty of fabrication.

Recently, waveguide-based microscopy that confines the guided light using a high refractive index material on a silicon (Si) chip, has attracted more and more interest due to its low cost, high compatibility with capability to be integrated with existing circuit design and fabrication processes. The subwavelength evanescent field on the top of the waveguide offers a uniform illumination to the sample, which extends over a wide FOV only limited by the attenuation of the light in the waveguide. The waveguide-based evanescent field excitation fluorescence microscopy decouples the illumination and detection paths [10–13], significantly reduces the complexity of the optical imaging system, demonstrating the advantages of high integration, large FOV and high-throughput. Most of the above-mentioned benefits of waveguide-based microscopy have been achieved by fluorescently labeled super-resolution imaging [14–18], while label-free super-resolution imaging on-chip without distortion has rarely been reported [19, 20]. Thus, a novel waveguide design enabling label-free reconstructed super-resolution images with high fidelity would be a significant breakthrough for the demands of many different technology scenarios.

Previous work simulated the light propagating process and imaging process based on a waveguide chip, indicating the super-resolution imaging capability with a high contrast-to-noise ratio (CNR) [21]. Here, we experimentally demonstrate a silicon nitride (Si_3N_4) waveguide-based label-free imaging system with tunable multi-wavelength illuminated spatial frequency shift (SFS) approach. This method eliminates the image distortion artifacts and realizes a high-fidelity super-resolution image reconstruction. Compared to other waveguide materials, Si_3N_4 material has a refractive index of about 2 in the visible spectrum to ensure super-resolution imaging, and the moderate refractive index contrast waveguide formed by oxide cladding can balance the bending radius and the waveguide loss. Low auto-fluorescence effect and low propagation loss create a clear background with large FOV. Additionally, the mature processing technology for Si_3N_4 make it an ideal material for low-loss waveguide-based SFS super-resolution imaging [22, 23]. In our work, an octagon waveguide working region is designed to be connected by eight input channels on each side of it, ensuring omnidirectional spatial frequency spectrum acquisition. The tunable SFS method is realized by coupling with three different wavelength illuminations in sequence to generate sub-images with multiple SFS components. The interaction of the evanescent wave illumination along different channels with the sample provides broad and complete spectrum information. In general, our SFS method can acquire separate all-directional spectrum

components with different illumination wavelengths, which is key to successful reconstruction without distortion using the iterative G-S algorithm. Compared with other SFS methods, the nanowire ring fluorescence illumination method lacks precise control of evanescent illumination direction, the sample will mix omnidirectional high wave vector components together, which makes it difficult to separate different frequency spectra in reconstruction [24–26]. The super-condenser nanoscopy method has also been used in conjunction with Si_3N_4 waveguide, while the generated Fourier ptychography reconstructions are found to be prone to image artifacts. With the sacrifice of resolution, a rotating coherent scattering algorithm is applied to counter reconstruction artifacts [20]. Our single-mode waveguide design demonstrates label-free super-resolution imaging capability for complicated random sample imaging with high-fidelity reconstruction owing to the more reliable mode control. Meanwhile, its compatibility with current complementary metal-oxide-semiconductor technology shows the potential of making a real mass-producible and compact super-resolution imaging chip.

To demonstrate the applicability of the Si_3N_4 waveguide for label-free super-resolution imaging, we visualized the etched three-slots structure and randomly distributed polymer beads. This is the first report that shows the waveguide-based label-free super-resolution imaging capability of complex random samples to our best of knowledge. The final reconstructed results agreed well with scanning electron microscopy (SEM, Zeiss Ultra 55 attached Oxford EDS Inca Energy Coater and QuoruTechnologies Sputter coater) images.

2. Method and chip fabrication

2.1. Imaging principle

The basic mechanism of the tunable SFS label-free super-resolution imaging is shown in figure 1(a). In the SF domain, the finer detail represents higher SF information, only diffraction-limited information can be transmitted to the far-field, leaving a high SF component bound to the object's surface in the form of evanescent waves [27]. A conventional microscope imaging system can be seen as a low pass filter in SF's perspective. The detectable SF domain is limited to a black circle with a radius of $k_0 = \frac{2\pi \times NA}{\lambda}$, where NA is the numerical aperture of the objective lens and λ is the wavelength of vertical illumination light. When evanescent field illumination with a large transverse wave vector $k_{eva} = \frac{2\pi \times n_{eff}}{\lambda}$ (n_{eff} is the effective refractive index of the waveguide mode) interact with sample, the maximal detectable SF of the samples are shifted to $k'_c = |-k_{eva}| + k_0$. Under different laser sources (wavelength) coupling in sequence, a variety of sample's frequency shift components are acquired to extend the regions in K space. Oblique illumination is also applied to fill up the bandgap between the vertical illumination and evanescent illumination. A full coverage of frequency information detection are accessible by changing the illumination direction along the channel of the waveguide.

To experimentally validate the tunable multi-wavelength super-resolution method, self-built microscopy (Thorlabs,
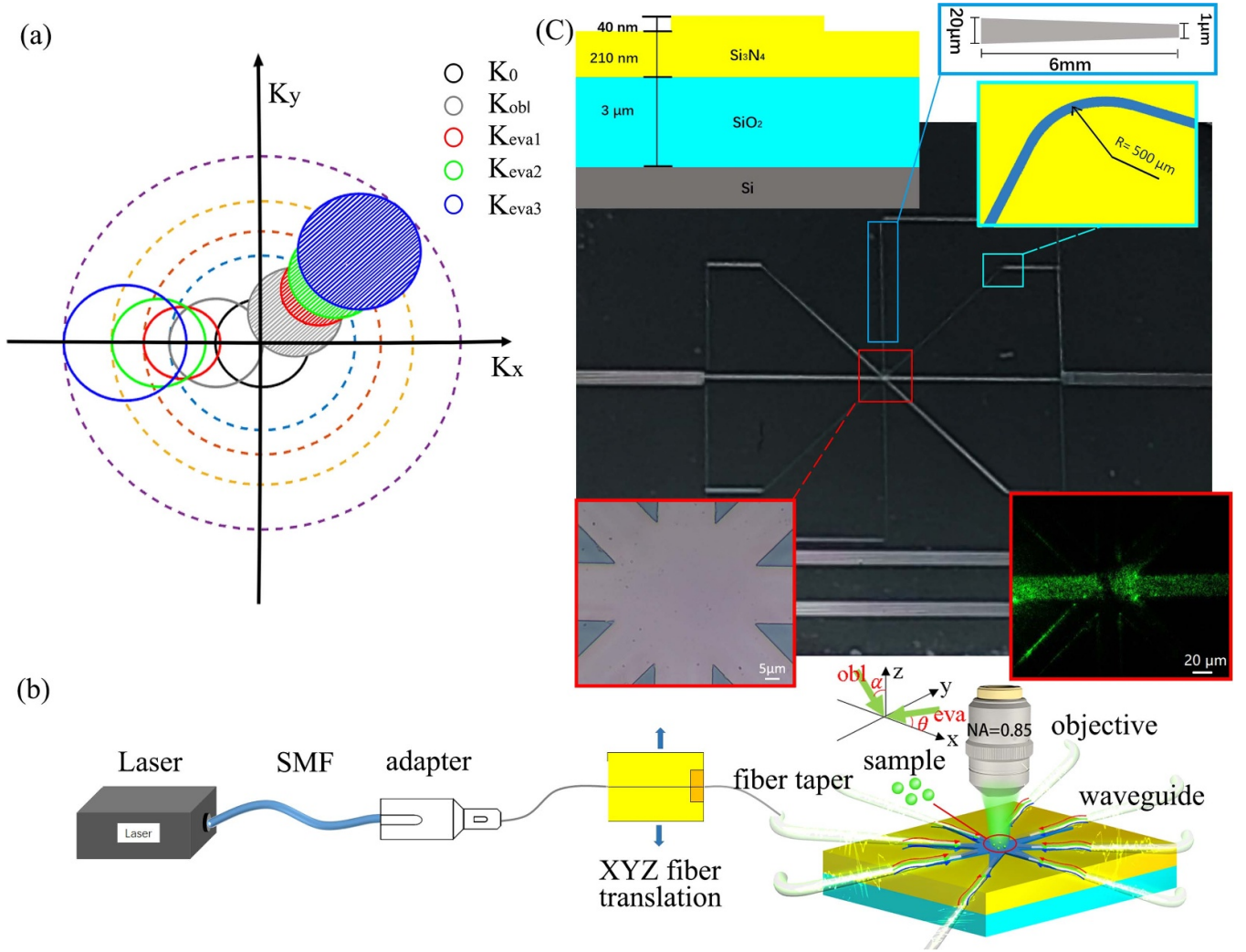
Figure 1. Schematic and mechanism of the Si_3N_4 waveguide-based super-resolution chip. (a) The basic mechanism of the multi-wavelength super-resolution label-free imaging. K_0 is the cutoff wave vector of the conventional microscopy. K_{obl} is the wave vector under oblique illumination. K_{eva1}, K_{eva2}, K_{eva3} are the corresponding wave vector of the three illuminating wavelengths. The purple dashed circle represents the maximal SF domain. (b) Schematic of the set-up and evanescent field illumination imaging process. Multiple directions frequency shifting information was obtained by changing the connection of different micro-fiber coupler one by one. Repeat this step after changing different evanescent illumination. θ represents the evanescent illumination angle with x-axis in the waveguide plane and α represents the angle between the oblique illumination and the z-axis. (c) The physical map of the overall layout of Si_3N_4 waveguide on Si chip. Side view of waveguide structure design based on shallow rib structure in the top-left. To maintain the single-mode conditions and broaden the imaging view, bending structure and adiabatically tapering were designed (top-right). And the illustration in the bottom-left corner shows the eight inputs working region under a bright-field optical microscope. Evanescent field illumination with high concentration scattering particles is shown in the bottom-right.

user-configurable cerna® mini microscopes) with a $100\times$ objective lens (Olympus, 0.85 NA), and a color CCD (Nikon DS-Filc, 3.45 μm pixel size) were used as our setup, as shown in figure 1(b). Eight micro-fibers are attached along the channels of the waveguide as couplers. A laser couples light into the single-mode fiber (Nufern, PM460-HP) as the illumination source and connects to one end of a micro-fiber. The evanescent field excited on the surface of the waveguide generates a scattered signal which is collected by the objective lens. Different directions frequency shifting information was obtained by changing the connection of different micro-fiber couplers one by one. Multi-wavelength lasers (Laseray-650 nm, 532 nm and 405 $nm^{-1} \sim$ 100 mW) were also coupled successively

to extend the collectable spatial frequency region. After the acquisition of intensity images of the sample under oblique and evanescent illumination, a G-S iterative reconstruction algorithm was utilized to recover the high-resolution image by updating functions back and forth between the real and Fourier spaces [28, 29].

Before the reconstruction procedure, we first align the intensity images using the edge of the working area and crop them to the same size with eight directions overlap region. Second, we set the square root of the superposition of 650 nm intensity images as an initial guess, $\sqrt{I_o}e^{i\varphi_0}$, where $\varphi_0=0$. From the Fourier transform of the initial guess, we will get a broad spectrum. Third, we select a subregion of this spectrum

J. Phys. D: Appl. Phys. **54** (2021) 315101

D Ye *et al*

and apply an inverse Fourier transform to get a new image, $\sqrt{I_1}e^{i\varphi_1}$. Fourth, we update the amplitude component $\sqrt{I_1}$ with the square root of obtained intensity images following from low wave vectors to large wave vectors $\sqrt{I_{new}}e^{i\varphi_1}$, and replace the corresponding subregion of the spectrum Fourier transform by the updated image. Finally, we repeat steps 3 and 4 to traverse all illuminations until the error curve between measured and estimated images tend to flatten. In this way, we can recover the targeted high-resolution image from Fourier space to the spatial domain.

This method satisfies 35% spectrum overlap to reconstruct the high-resolution image. Conventional illumination ($\lambda = 405$ nm) with 0.85 NA objective lens offers a maximal resolution of $\lambda/_{2NA} \approx 238$ nm. The chip-based multi-wavelength SFS super-resolution method offers a maximal resolution of $\lambda/_{(NA + n_{eff})} \approx 142$ nm (corresponding $n_{eff} \approx 2$). By choosing a high refractive index of the material, the resoluition is improved 1.676 times.

2.2. Chip fabrication

In the visible regime, the single-mode condition requires the width of the waveguide to be hundreds of nanometers, requiring complicated and expensive nanoscale processing such as electron-beam lithography. The rib geometry waveguide structure makes it possible for single-mode propagation with a relatively wider waveguide [16, 30]. Combining with waveguide bending to filter the high order modes and adiabatically tapering of the rib waveguide for large FOV, a 1 μm wide single-mode waveguide could be realized.

First, the Si_3N_4 waveguide was fabricated by growing a silica layer with a thickness of 3 μm on a silicon wafer to offer a moderate index contrast, which renders the waveguiding mechanism less prone to scattering losses associated with the waveguide sidewall roughness [31]. Two hundred and fifty nanometer thick Si_3N_4 layer was deposited using low-pressure chemical vapor deposition at 800 °C, enabling a strong waveguide surface evanescent field. After preparation of the planar waveguide, the preset photoresist mask for the waveguide was patterned using standard photolithography. Finally, the pattern was transferred into the Si_3N_4 layer using reactive ion etching (RIE) to fabricate the rib waveguides with 1.829 dB cm^{-1} transmission loss. The etching depth is set as 40 nm, considering the limited processing condition and etching accuracy. The cross-section of the waveguide as shown in figure 1(c) top-left. Bending structures (bending radius = 500 μm) and 6 mm long adiabatically tapered zones are performed to maintain single-mode conditions (top-right corner in figure 1(c)), creating the effective overlap viewing area around 400 μm^2. 100× optical microscope measurement indicated no obvious scattering points in the octagon viewing area (bottom-left corner in figure 1(c)). When the single mode is excited in a low loss waveguide, the light intensity will be uniform along with the waveguide's long distance. To experimentally demonstrate this, we have dropped a high concentration particulate solution (FluoSphere carboxylate-modified, diameter 0.1 μm, red (580/605 nm), 1:10 dilution ratio) on the waveguide, and

the scattered light on the waveguide surface is almost uniform as shown in the bottom-right corner of figure 1(c).

3. Results and analysis

3.1. Simulation using different illumination field distributions

The uniform illumination field and unidirectional propagation properties along the waveguide structure are key factors to the high fidelity image reconstruction. We simulated the field interaction process between object and evanescent field as shown in figure 2 with different incident field distributions. The slots deposited on the waveguide surface are 70 nm wide and spaced 70 nm apart shown in Figures 2(a) and (e). With oblique and evanescent wave illuminating perpendicularly to the slots, the scattered signals are collected under 0.85 NA objective lens and reconstructed by G-S algorithm. As shown in figure 2(b), the uniform light field input into one side of waveguide channels is confined to a narrow range of angle. Figures 3(c) and (d) shows the perfect low resolution image and accurate reconstruction. When the illumination field excites high modes in figure 3(f), the low-resolution image suffers severe information loss and the distorted reconstruction result is shown in figures 3(g) and (h).

3.2. Experimental results and analysis

To test the practical performance of our waveguide chip, we fabricated a three-slots structure with different periods (the center to center distance between adjacent slot is 175 nm and 160 nm, from up to down) using focused ion beam. Figure 3(a) shows the SEM image of etching structure on the working region of Si_3N_4 waveguide. Firstly, vertical and oblique lights are applied to illuminate the sample. Corresponding images are shown in figures 3(b) and (c), respectively. The setup of our oblique illumination system consists of a supercontinuum source (YSL Photonics' SC-OEM, central wavelength is set to 532 nm) and an electric controlling two 1D Galvo Mirror (GM) system. Incident angles of oblique illumination are precisely controlled by GM. Afterwards, evanescent field illumination with 650 nm, 532 nm, and 405 nm wavelength is coupled with tapered single-mode fiber, and multi-wavelength evanescent imaging could realize by changing different color laser sources after accurately attaching the micro-fiber to respective channels. The images under different illuminations are obtained using a 100× objective lens (0.85 NA, work distance $d = 3.4$ mm) and a color CCD with a pixel size of 31 nm at the object plane (CCD pixel size divided by the magnification factor). As shown in figures 3(b)–(i), under vertical, oblique and evanescent illumination, low-frequency, mid-frequency and high-frequency information of the sample can be excited and captured. However, no image shows the real size and structures of the sample under any kind of illumination.

During the reconstruction process, we first aligned the captured intensity images ($4 \times 2 + 1$) using the edge of the working area and cropped them to the same size (208×208 pixels each) by the overlapped region of light fields propagating from different directions. Next, the phase recovery G-S algorithm
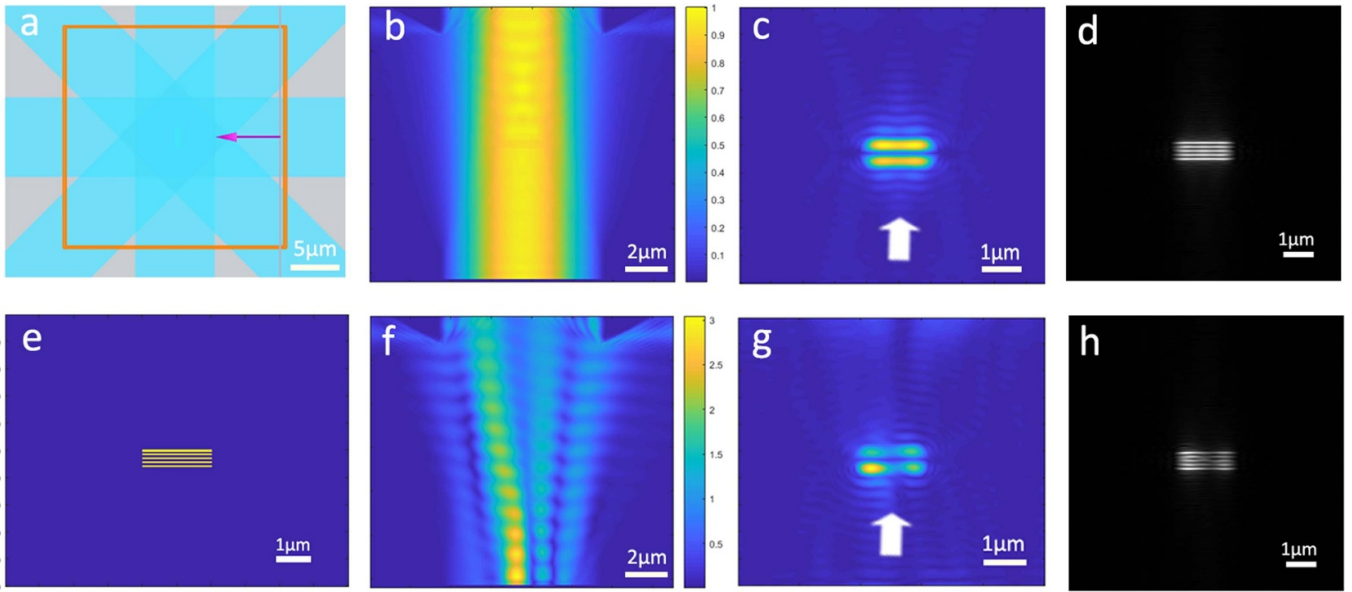
Figure 2. Simulation of illumination field distribution influence in reconstruction. (a) Simulated octagon area with slots structure. (b) Single-mode field distribution in the waveguide under 650 nm. (c) Image under evanescent illumination at a wavelength of 650 nm. (d) The reconstructed high-resolution image with single-mode illumination. (e) Simulated test sample comprising 70 nm wide and 70 nm apart. (f) High modes field distribution in the waveguide under 650 nm. (g) Image under evanescent illumination at a wavelength of 650 nm. (h) The reconstructed high-resolution image with high-modes illumination.
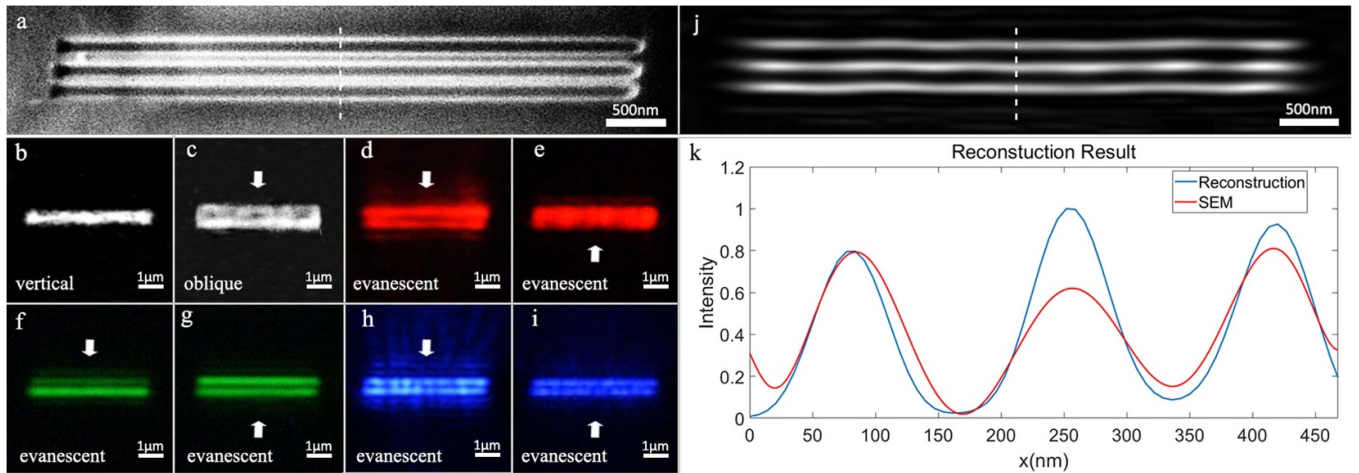

Figure 3. (a) SEM image of a structure with three-slots. The center-to-center distance between the adjacent slot is 175 nm and 160 nm (from up to down) (b) optical image of the structure obtained under vertical illumination. (c) Image with oblique illumination incident at $\alpha = 45°$ and travelling along a direction defined by white arrow. (d), (e) Images under evanescent illumination at a wavelength of 650 nm. (f), (g) Images under evanescent illumination at a wavelength of 532 nm. (h), (i) Images under evanescent illumination at a wavelength of 405 nm. The arrows represent corresponding propagation directions of illumination. (j) Reconstructed image. (k) Intensity profiles along the white dash line in (a) and (j).

was utilized to shift the different illumination wave vectors sub-images SF spectrum to the correct position of the original spectrum of the sample. With ten times iteration, a converged reconstruction result with enough CNR in the spatial domain is shown in figure 3(j). We randomly measured the intensity profiles along the feature points both in the reconstruction result and SEM image. Figure 3(k) shows the intensity profiles along the white dashed lines indicated in figures 3(a) and (j). The center-to-center distance at two points equal to the number of pixels between two points' peaks of intensity multiplied

by the actual distance represented by each pixel. And the distance error between the reconstruction result and SEM image is under 10%, which demonstrates good agreement between our experimental results and the SEM image.

After the etched structure imaging verification, we applied our super-resolution chip to randomly distributed polymer spheres (FluoSphere carboxylate-modified, diameter 0.1 μm, red (580/605 nm)) imaging. The sample was diluted using deionized water with a ratio of 1:1000 and dispersed with ultrasonication for 5 min. The solution was dropped on the
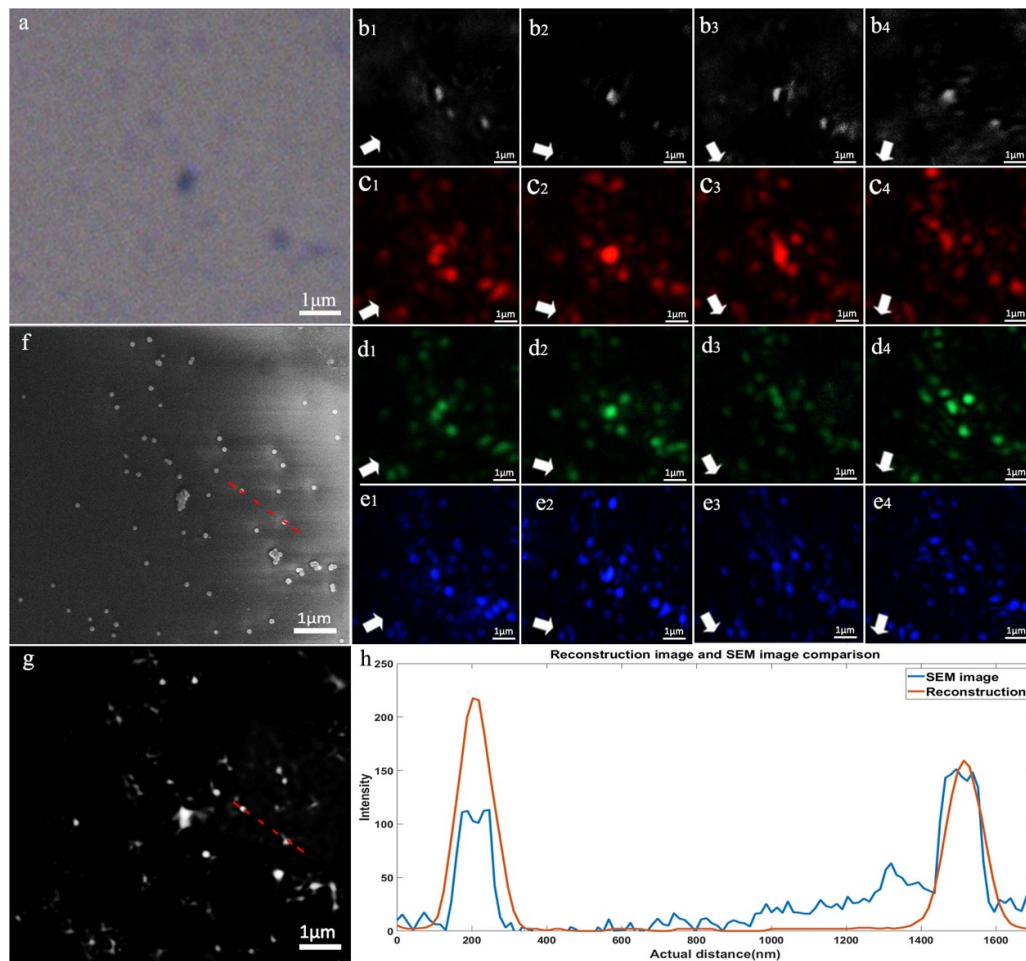
Figure 4. (a) Optical image of polymer spheres obtained under vertical illumination. (b) Different images with oblique illumination incident at $\alpha = 45°$ and travelling along a direction defined by white arrow. (c)–(e) Images under different evanescent illumination incident θ at a wavelength of 650 nm, 532 nm, and 405 nm. The white arrows represent corresponding propagation directions of illumination. (f) SEM image of polymer spheres randomly distributed on the waveguide surface. (g) Final reconstructed image. (h) Intensity profiles along the red dash line in (f) and (g).

surface of the waveguide and heated for 5 min after spontaneous evaporation. Figure 4(f) shows a SEM image of one region on the chip. As demonstrated in figure 4(a), the same region captured by conventional bright-field microscope can only recognize mass agglomerated particles because of low resolution and low CNR. Part of the oblique and evanescent illumination (650 nm, 532 nm, and 405 nm) images along the direction of the white arrow are demonstrated in figures 4(b)–(e), respectively. Note that the scattered signal is wavelength-dependent and angular-dependent, which seriously affects the CNR of the images despite adjusting the exposure time of the camera. After cutting and aligning with feature points, a stack of preprocessed images ($4 \times 8 + 1$) with 300×300 pixels were utilized to reconstruct a high-resolution image by iteration algorithm, as shown in figure 4(g). The reconstruction result with 600×600 pixels demonstrated a definite resolution improvement and CNR of the image gets an increase from 27.4 to 138.8 after performing the reconstruction algorithm. Figure 4(h) shows the red dashed lines indicated in figures 4(f), (g) and demonstrates good agreement with the SEM image. However the reconstruction-related artifacts appear by

using noise-corrupted raw sub-images especially in fine structure.

There are two main reasons for this. First and foremost, evanescent illumination light excited by the waveguide is based on the micro-nanofiber evanescently coupling method. The short mode filter distance results in residual high modes excited by the wide waveguide channel. The superposition of these high order modes along the waveguide causes the non-uniform evanescent illumination. Some sample details are missing under the uneven illumination, which seriously affects the final reconstructed image quality. Secondly, the polymer spheres will inevitably aggregate during solution preparation and excite a strong scattered signal. Suppressing their over-exposure may cause some scattered signals drowned out by noise. Also, the wavelength-dependent and angular-dependent character of the scattered signal seriously impact the image CNR, which makes the iteration algorithm a big challenge in eliminating reconstruction artifacts.

In order to solve the problems in the experiments, we simulated the imaging process of the randomly distributed polymer spheres with 100 nm diameters, as shown in figure 5(a). A 0.85

J. Phys. D: Appl. Phys. **54** (2021) 315101

D Ye *et al*
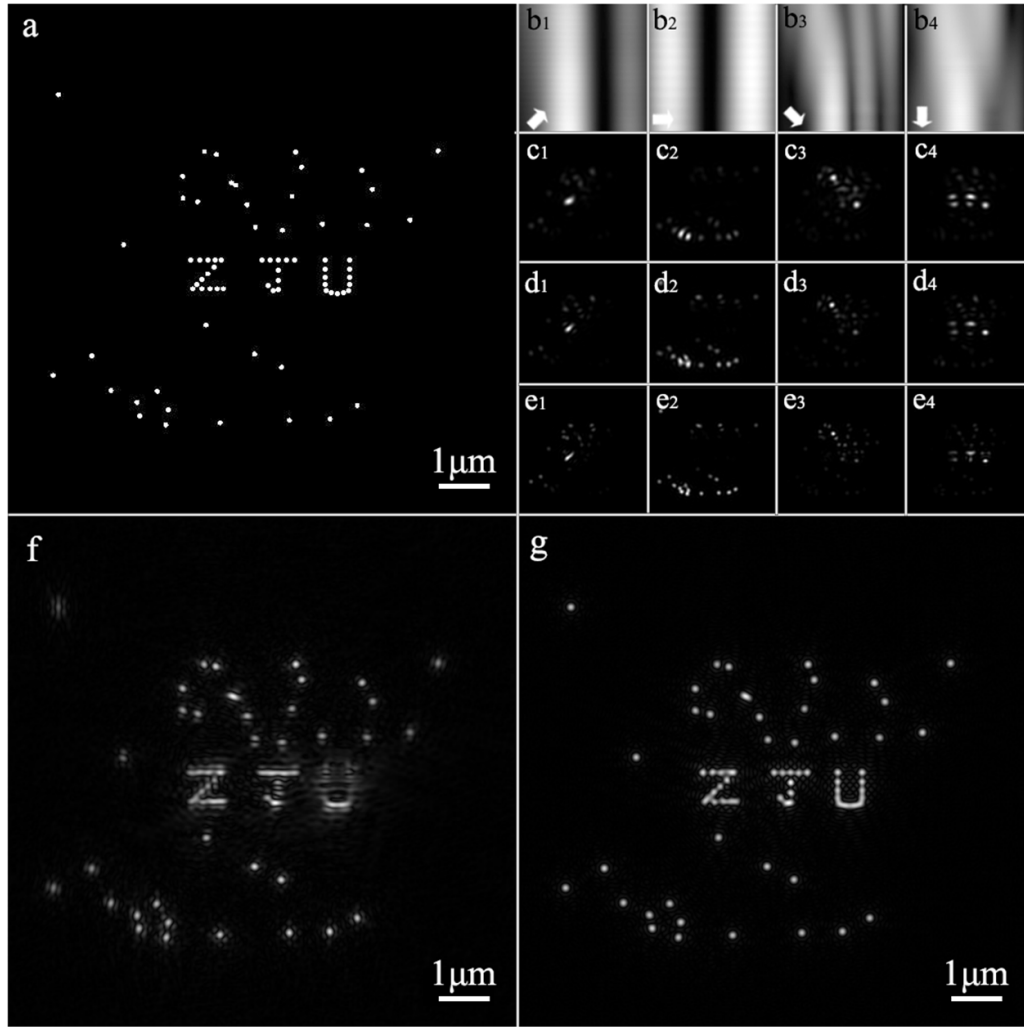
Figure 5. (a) Simulated scattered spheres with 100 nm diameter. (b) Multi-mode illumination input into different directions. (c)–(e) Evanescent illumination sub-images with 650 nm, 532 nm, 405 nm in the corresponding directions. (f) Final reconstruction image. (g) The modified result with the averaged mode distribution.

NA objective lens was used to collect scattered light in the far-field. As shown in figure 5(b), non-uniform evanescent field illuminations input into the channels along with different directions respectively. The corresponding sub-images demonstrated a distinct inhomogeneous intensity in figures 5(c)–(e). Some details were missing, resulting in incomplete reconstruction in figure 5(f). Densely distributed 'ZJU' pattern suffered from a serious reconstruction failure while the randomly distributed spheres around showed high position accuracy, which fit well with the experimental phenomenon. Here we simulated the mechanical motion of the butt coupling objective lens back and forth to obtain an average mode distribution of all-direction sub-images. As a result, the structural information is clearly reconstructed in figure 5(g). The best resolution measured in the modified result is 160 nm, slightly below the theoretical limit resolution (about 142 nm).

Uneven illumination may bring about severe missing spatial frequency information, but still can resolve the message we have gotten using the reconstruction algorithm. Also, different mode patterns superposition can perfectly solve the

problem and obtain a complete reconstructed super-resolution image. In the future, more mature chip process technology could promote a guarantee of high-performance single-mode condition waveguide chips. Furthermore, an advanced frequency reconstruction algorithm will be developed to further eliminate the reconstruction artifacts.

4. Conclusion

In conclusion, we developed a label-free SFS super-resolution imaging based on an Si_3N_4 waveguide. Using conventional lithography and RIE technology, a quasi single-mode rib waveguide with an octagonal viewing area was fabricated. Through sequentially coupling three illuminating wavelengths from different directions, the evanescent wave of the propagation mode successively interacts with the sample to shift different high SF domains into enabling detection range with SFS effect. Combining with vertical, oblique and evanescent illumination, multiple spatial frequency information was

J. Phys. D: Appl. Phys. **54** (2021) 315101

D Ye *et al*

obtained and high-resolution images without distortion were reconstructed using the G-S iteration algorithm. We introduced the SFS method to image the etched three-slots structure and polymer beads. All of them match well with SEM images, demonstrating great potential for biomedicine, materials science, and defect detection [32].

For further improvement of the integration and compactness of our super-resolution chip, the integrated electroluminescent broadband LED film will be utilized. Additionally, suitable waveguide materials with higher refractive index, such as GaP and SiC, could allow the resolution to reach less than 100 nm. Plasmonic excited high frequency light field mixing with structure illumination modulation provides a new perspective for coherent super-resolution imaging [33]. Furthermore, the waveguide structure design is also suitable for fluorescently labeled super-resolution imaging loading of interference angle tunable SIM [34, 35], demonstrating the capacity for label and label-free imaging compatibility.

Data availability statement

The data generated and/or analysed during the current study are not publicly available for legal/ethical reasons but are available from the corresponding author on reasonable request.

Acknowledgments

ORCID iD

Qing Yang ⬥ https://orcid.org/0000-0002-9609-558X

References

[1] Pendry J B *et al* 2000 *Phys. Rev. Lett.* **85** 3966–9
[2] Fang N, Lee H, Sun C and Zhang X 2005 *Science* **308** 534–7
[3] Huang T, Yin L, Zhao J, Du C and Liu P 2019 *ACS Photonics* **7** 2173–81
[4] Smolyaninov I I, Hung Y J and Davis C C 2007 *Conf. on Lasers & Electro-optics-pacific Rim Science* vol 315 pp 1699–701
[5] Lee D *et al* 2018 *ACS Photonics* **5** 2549–54
[6] Huang T, Tang H, Tan Y, Li L and Liu P 2019 *IEEE Trans. Antennas Propag.* **67** 3358–65
[7] Wang Z, Guo W, Li L, Yanchuk B L, Khan A, Liu Z, Chen Z and Hong M 2011 *Nat. Commun.* **2** 218
[8] Fabrice L, Geoffroy L, Julien D R and Mathias F 2010 *Phys. Rev. Lett.* **104** 203901
[9] Rogers E T F, Lindberg J, Roy T, Savo S, Chad J E, Dennis M R and Zheludev N I 2010 *Nat. Mater.* **11** 432–5
[10] Grandin H M, Städler B, Textor M and Vörös J 2006 *Biosens. Bioelectron.* **21** 1476–82
[11] Hassanzadeh A, Nitsche M, Mittler S, Armstrong S, Dixon J and Langbein U 2008 *Appl. Phys. Lett.* **92** 233503
[12] Agnarsson B, Ingthorsson S, Gudjonsson T and Leosson K 2009 *Opt. Express* **17** 5075–82
[13] Agnarsson B, Jonsdottir B, Arnfinnsdottir N B and Leosson K 2011 *Opt. Express* **19** 22929–35
[14] Agnarsson B, Lundgren A, Gunnarsson A, Rabe M, Kunze A, Mapar M, Simonsson L, Bally M, Zhdanov V P and Höök F 2015 *ACS Nano* **9** 11849–62
[15] Diekmann R, Helle Ø, Øie C, McCourt P, Huser T, Schüttpelz M and Ahluwalia B S 2017 *Nat. Photon.* **11** 322–8
[16] Tinguely J C, Helle Ø I and Ahluwalia B S 2017 *Opt. Express* **25** 27678–90
[17] Archetti A, Glushkov E, Sieben C, Stroganov A, Radenovic A and Manley S 2019 *Nat. Commun.* **10** 1267
[18] Helle Ø I, Dullo F, Lahrberg M, Tinguely J C, Ahluwalia B S and Hellesø O G 2020 *Nat. Photon.* **14** 431–8
[19] Pang C *et al* 2019 *Adv. Funct. Mater.* **29** 1900126
[20] Ströhl F, Opstad I S, Tinguely J C, Dullo F, Mela L, Osterrieth W M, Ahluwalia B S and Clemens C F 2019 *Opt. Express* **18** 25280–92
[21] Xu X, Liu X, Pang C, Ma Y, Meng C, Zhang J, Liu X and Yang Q 2019 *J. Phys. D: Appl. Phys.* **52** 28
[22] Gorin A, Jaouad A, Grondin E, Aimez V and Charette P 2008 *Opt. Express* **16** 13509–16
[23] Muellner P, Melnik E, Koppitsch G, Kraft J, Schrank F and Hainberger R 2015 *Proc. Eng.* **120** 578
[24] Hao X, Liu X, Kuang C, Li Y, Ku Y, Zhang H, Li H and Tong L 2013 *Appl. Phys. Lett.* **102** 013104
[25] Pang C *et al* 2017 *Opt. Lett.* **42** 004569
[26] Liu X *et al* 2017 *Phys. Rev. Lett.* **118** 076101
[27] Tang M, Liu X, Wen Z, Lin F, Meng C, Liu X, Ma Y and Yang Q 2020 *Laser Photon. Rev.* **11** 1900011
[28] Gerchberg R W and Saxton W O 1972 *Optik* **35** 237–50
[29] Zheng G, Horstmeyer R and Yang C 2013 *Nat. Photon.* **7** 739–45
[30] Dullo F, Tinguely J, Solbo S and Helleso O 2015 *IEEE Photon. J.* **7** 2387252
[31] Dabos G, Manolis A, Giesecke A L, Porschatis C, Chmielak B, Wahlbrink T, Pleros N and Tsiokos D 2017 *Opt. Commun.* **10** 1016
[32] Glushkov E *et al* 2019 *ACS Photonics* **6** 3100–7
[33] Fernández-Domínguez A I, Liu Z and Pendry J B 2015 *ACS Photonics* **2** 150129105221000
[34] Liu X, Meng C, Xu X, Tang M, Pang C, Ma Y, Shi Y, Yang Q, Liu X and Kaminski C F (arXiv:1906.11647)
[35] Tang M *et al* (arXiv:2103.09321)